Energy Conversion and Management: X 16 (2022) 100296

Contents lists available at ScienceDirect

Energy Conversion and Management: X

journal homepage: www.sciencedirect.com/journal/energy-conversion-and-management-x

Experimental and thermodynamic analysis of solar air dryer equipped with V-groove double pass collector: Techno-economic and exergetic measures

Ali Hassan [a], Ali M. Nikbahkt [a], Zachary Welsh [a], Prasad Yarlagadda [a], Sabrina Fawzia [b], Azharul Karim [a,*]

[a] School of Mechanical, Medical and Process Engineering, Queensland University of Technology, Brisbane, Australia
[b] School of Civil and Environmental Engineering, Queensland University of Technology, Brisbane, Australia

ARTICLE INFO

Keywords:
V-groove
Solar dryer
Exergy
Specific energy consumption
Drying rate

ABSTRACT

Optimised solar air dryers, in terms of efficiency and performance, can solve some major concerns in the agro-industrial processing sector. Solar air dryers can reduce the large share of energy costs of a final product and can provide sustainable energy in rural areas where access to energy is often limited. In this study, a pilot scale v-groove double pass solar air collector has been analysed thermodynamically with real time solar radiation and mass flow rate (0.021–0.061 kg/s) inputs and validated experimentally in terms of first and second law efficiencies. Performance of the process was assessed using experimental drying measures including final moisture content, drying rate and exergy efficiency for drying of Pink Lady apples. Energy payback time and specific energy consumption were calculated to reveal the techno-economic value of the system. The maximum thermal efficiency of the collector was observed to be 88.8 % at 0.061 kg/s having exergy efficiency of 6.6 % which shows an efficient sourcing for the operation. In terms of the performance of the dryer, mass flow rate of 0.041 kg/s offers a higher moisture removal. Specific energy consumption (*SEC*) was 3.096 kWh/kg. Thermodynamic model was validated with matching experimentation with acceptable RMSE for the range of investigated measures. Energy payback period time calculated by the embodied energy of the system was obtained to be 0.78 years which implies that the system is capable of addressing a large capacity drying if it is to be scaled-up.

1. Introduction

Global warming and food security have been two major concerns in the agri-food industry over the last few decades. The food industry accounts for 30 % of the total global greenhouse gas emissions [1] and it is estimated that around 1.3 billion tons of food is wasted worldwide yearly contributing directly and indirectly to global warming in terms of greenhouse gas emissions, air and water pollution and deforestation [2,3]. One solution to trivialize the global warming and greenhouse gas emissions from the agri-food industry is to minimize the food waste by enhancing the shelf life using proper preservation techniques, i.e. drying [4].

Drying can reduce the water activity while maintaining the product quality and nutritional value [5]. However, drying is an energy intensive process and comprises 15 % of the total industrial energy consumption of the sector [6,7]. Over the years there has been several drying techniques developed, such as microwave, vacuum drying, spray drying, infrared, heat pump assisted drying, convective drying and freeze drying [8]. Although all these drying technologies reduce fresh food waste by enhancing the product shelf life, each have their own advantages and disadvantages depending on the scenario [9]. Additionally, one key disadvantage of many of these drying techniques is their contribution towards greenhouse gas emissions. Solar drying on the other hand does not contribute towards a dryers emissions and uses solar radiation to dry the fruits and vegetables either directly or by using a solar air collector for forced convective drying [10]. Direct solar drying has no adverse effect on the environment, however it has some considerable disadvantage in terms of extensive dehydration time, small foodstuff capacity and quality [11]. Solar air dryer is more efficient compared to direct solar drying due to its ability to reduce the dehydration time and specific energy consumption. However, solar dryers suffer from intermittency of solar radiation and hence the performance is affected. To overcome the intermittency in the solar radiation and ensure the continuous drying operation, an efficient thermal storage system is required [12,13]. Nano fluids are also used to improve the performance of thermal storage [14,15].

To enhance the performance of solar air dryers, optimizing the

* Corresponding author.
E-mail address: azharul.karim@qut.edu.au (A. Karim).

https://doi.org/10.1016/j.ecmx.2022.100296
Received 3 August 2022; Received in revised form 2 September 2022; Accepted 3 September 2022
Available online 9 September 2022

Nomenclature

A	Area of Collector (m^2)
x	Insolation thickness (m)
D_h	Hydraulic diameter (m)
C_p	Specific heat constant $\left(\frac{kJ}{kg\,K}\right)$
$\dot{m}$	mass flow rate of air $\left(\frac{kg}{s}\right)$
Nu	Nusselt number
Re	Reynold number
U_F	Air velocity $\left(\frac{m}{s}\right)$
H_{groove}	Height of v-groove (m)
N_G	Number of glass covers
I	Solar Radiation $\left(\frac{W}{m^2}\right)$
T_o	Outlet air temperature (°C)
T_{Fi}	Air inlet temperature (°C)
T_A	Ambient Temperature (°C)
T_P	Plate Temperature (°C)
T_G	Glass Temperature (°C)
T_{F1}	Fluid first pass temperature (°C)
T_{F2}	Fluid second pass temperature (°C)
T_B	Bottom Plate Temperature (°C)
$T_{i,\,DC}$	Dryer inlet temperature (°C)
$T_{o,\,DC}$	Drying chamber outlet temperature (°C)
T_s	Sun temperature (°C)
T_e	Environment temperature (°C)
h	Enthalpy $\left(\frac{kJ}{kg}\right)$
$\dot{Q}_s$	Useful heat gain (W)
k	Thermal conductivity $\left(\frac{W}{mK}\right)$
s	Entropy
$h_{c,G-F}$	Convective heat transfer coefficient glass to fluid $\left(\frac{W}{m^2K}\right)$
$h_{c,\,P-F}$	Convective heat transfer coefficient plate to fluid $\left(\frac{W}{m^2K}\right)$
$h_{r,P-B}$	Radiation heat transfer coefficient absorber to back plate $\left(\frac{W}{m^2K}\right)$
$h_{r,G-A}$	Radiation heat transfer coefficienct glass to ambient $\left(\frac{W}{m^2K}\right)$
$h_{r,P-G}$	Radiation heat transfer coefficient plate to glass $\left(\frac{W}{m^2K}\right)$
h_w	Wind heat transfer coefficient $\left(\frac{W}{m^2K}\right)$
U_T	Overall heat loss coefficient $\left(\frac{W}{m^2K}\right)$
U_B	Backplate heat loss coefficient $\left(\frac{W}{m^2K}\right)$
U_T	Top loss heat coefficient $\left(\frac{W}{m^2K}\right)$
U_E	Edge loss heat coefficient $\left(\frac{W}{m^2K}\right)$
Ex	Exergy
Ex_{dest}	Exergy destruction
m_I	initial mass (kg)
m_d	dried mass (kg)
m_w	mass of evaporated water (kg)
E_{in}	Energy inlet to the dryer
$M.C_{wb}$	Moisture content wet basis
M_t	Total moisture content (%)

Greek Letters

η	Thermal efficiency (%)
η_{II}	Exergy efficiency (%)
ε_P	Plate emissivity
ε_G	Glass emissivity
α_G	Glass absorptivity
α_P	A bsorber absorptivity
τ	Glass transmissivity

Abbreviations

SEC	Specific energy consumption
IP	Improvement potential
DC	Drying Chamber
SI	Sustainability index

operating conditions and design of their solar air collector is necessary. Sun et al. [16] numerically analysed the operating conditions and performance of flat plate solar air heater and achieved maximum thermal efficiency around 55 % at the mass flow rate of 0.050 kg/s. Bagga et al. [17] recommended to use forced convection using flat plat solar air collector for drying purposes instead of natural convection. Similarly, Mahmood et al. [18] investigated various mass flowrates (0.011–0.032 kg/s) uncovering maximum thermal efficiencies of 62.50 % at the mass flow rate of 0.032 kg/s for double pass with transverse fins. Solar air collector performance can also be enhanced by optimizing the geometry of the absorber by employing fins [19–21], ribs [22–24], and baffles [25–27] on the absorber surface, replacing flat plate with v-groove [28,29], cross corrugated absorbers [30,31], increases the number of passes for air inside the solar air collector [31]. Abo-Elfadl et al. [32] found that double pass tubular solar air heater had superior performance in terms of first and second law efficiency, CO_2 mitigation and outlet air temperature compared to flat plate solar air heater. Hachemi et al. [19] analysed the performance of solar air collector integrated with staggered fins. Thermal efficiency was enhanced from 38.6 % (for flat plate collector) to 75.5 % using staggered fins with 10 cm length and 2.5 cm gap between staggered fin rows. El said et al. [26] numerically investigated the effect of perforated baffles on solar air collector performance. Around 77 % thermal efficiency was achieved at 3 mm diameter, 7° angle and 0.07 kg/s flow rate. Kalaiarasi et al. [33] achieved thermal efficiency of 59.02 % at 0.026 kg/s using flat plate with sensible heat storage (Therminal-55). Benhamza et al. [34] analysed solar air heater integrated with fins and achieved outlet temperature of 52 °C, and 51.78 % thermal efficiency, respectively. Using fins, ribs, and artificial roughness allows the heat transfer area and turbulence effect to increase. Concentrated solar collectors have also been studied for higher temperature applications [35,36]. The idea of increasing heat transfer rate of collectors may be impacted by high costs and precise machining due to increased surface area and addition of turbulators.

Alternatively, use of V-groove absorber provides an economical option with less cost and high thermal performance. Desisa and Shekata et al. [28] numerically achieved 90 %, 62 % and 78 % thermal efficiency for V-groove, flat plate, and rough plate solar air collector, respectively. Karim et al. [37,38] found that v-corrugated SAC had better thermal performance compared to flat plate and finned plate SAC. El-Sebaii et al. [30] found lower overall heat losses by using v-corrugated solar air heater with 14 % higher thermal hydraulic efficiency compared to flat plate solar air collector due to enhanced heat transfer area for v-corrugated absorber. Promvonge and Skullong et al. [39] found that V-ribs integrated with V-groove had better thermal performance compared to V-groove and solid V-rib solar air heater. Sudhakar et al. [40] enhanced the thermal efficiency up to 17.4 % using double pass V-groove integrated with pin-fins compared to a flat plate solar air heater. Sethi et al. [41] used single pass v-groove solar air heater for drying. Their results showed an energy efficiency of 73.3 % and 24.8 % for solar air collector and drying chamber. Lingayat et al. [42] achieved thermal efficiency of 54.5 % and 25.39 % for v-groove single pass solar air collector and drying chamber for apple drying, respectively. The literature has demonstrated in general that V-groove plates are low cost with high thermal efficiency designs compared to fins, ribs, and baffles.

Consideration of the thermal efficiency deduced from the first law of thermodynamics is a conventional and of course vital part of any

collector analysis, but does not give the perception of available work and irreversibilities which reduce the sustainability of the process [43]. Therefore, exergetic analysis of the process provides a practical sense of losses, irreversibility, optimising potential and availability of wasted energy streams [44]. Exergy is an indicator of how much useful energy is available to the system that can be directly utilized for certain application such as drying. Exergy efficiency is commonly lower compared to the thermal efficiency due to the entropy generated in the system by heat losses, pressure losses and frictional losses. In the literature, exergy efficiency was 5.2 % [22], 5.84 % [45] and 3.6 % [40] when baffle-fins, zig-zag copper tube SAH, and double pass integrated with pin fins were used, respectively. 55.28 %, 45.32 % and 58.14 % maximum exergy efficiency was achieved for the drying chamber [46 47 41]. Therefore, various work has been done on energy and exergy analysis of solar air collectors and solar air dryers, however the energy and exergy analysis of V-groove double pass solar air collector integrated with drying chamber for the drying applications is not available. The V-goorve double pass solar air collector has high thermal capabilities in terms of energy and exergy efficiency due to high heat transfer surface area of V-groove double pass absorber. High thermal performance makes it more suitable for drying application if it is integrated with a dryer.

The third globally accepted measure in the energy analysis of a system is the specific energy consumption (*SEC*) which in the dryer case, is simply defined as energy required for a unit mass of moisture evaporated. It is widely adopted in the literature to give comparison for several techniques. Sethi et al. [41] used single pass v-groove solar air collector for drying potato chips. Specific energy consumption was reduced by 13.08 % while specific moisture extraction rate was improved by 21.05 % using single pass v-groove collector compared to flat plate solar air collector. Tagne et al. [48] studied combined effect of natural and forced convection drying using indirect solar dryer for cocoa beans drying. Around 0.15 kg/kg db moisture content was achieved by employing forced convection for 24 h and by employing natural convection for 32 h with specific energy consumption between 5 and 15 kWh/kg. Tuncer et al. [49] used quadruple pass solar air heater integrated with greenhouse dryer for drying of red pepper and kiwi. Thermal efficiency and specific moisture extraction rate was found to be around 80.66 % and 0.21–0.36 kg/kWh. Rahman et al. [50] found that cell of the apple started to rupture when temperature was enhanced from 50 to 70 °C. Moussaoui et al. [51] used hybrid forced electric-solar dryer for drying apple peels. Specific energy consumption for drying apple peels was 12.2310 MWh/kg and 5.3072 MWh/kg at 50 °C and 80 °C, respectively. Romano et al. [52] found that energy required to dry the apple was around 3300.19 kJ/kg with final moisture content of 26 %. Therefore, it is evident that specific energy consumption (*SEC*) is a tangible measure for the amount of energy saved by solar air collectors giving an economic estimation in terms of electricity tariffs and energy payback period.

Assessing the economic characteristics of technologies early in their developmental trajectories can help technologists either efficiently accelerate emissions reductions and commercialization or realize potential infeasibility and direct resources toward better opportunities. Techno-Economic analysis (TEA) is defined as an assessment of the overall value (benefit and cost) of a technology. TEA provides basic assumptions and sources of information which identifies all the parameters that impact value and includes appropriate margins for uncertainty. There have been several documents published on techno-economic analysis of solar energy systems. Economic feasibility of indirect solar dryers is important for the industrial sustainability. Ekka et al. [53] evaluated the economic feasibility of forced convection mixed mode solar dryer for different fruits (jackfruit, ginger, turmeric and red chilli). Economic analysis showed payback period, internal rate of return and energy payback time of 0.9 years, 130 % and 3.75 years, respectively, with 8.4 tonne potential of CO_2 mitigation over the life cycle. Lakshmi et al. [54] had estimated the payback period of 0.65 years for drying stevia leaves using a mixed mode forced convection solar dryer. Hadibi et al. [55] used solar-geothermal dryer for drying of tomatoes with estimated payback period of 0.325 years and exergy efficiency of 54 %, respectively. Gupta et al. [56] developed a novel photovoltaic thermal solar dryer for star fruit drying. The estimated payback period was 1.4 year with the exergy efficiency of 31.12 % for forced convection drying. Singh et al. [57] used evacuated tubes as indirect solar dryer for drying of turmeric and fenugreek leaves with estimated payback period of 555 and 604 days, respectively.

In recent years, significant research has been conducted for performance analysis of indirect solar dryers such as single pass V-shaped, flat plate single pass and double pass, double pass with iron mesh, solar air heater with fins/ribs/baffles for drying of fruits and vegetables as discussed in the former paragraph. However, energy, exergy and economic analysis of V-groove double pass solar air collector with drying chamber have not yet studied to evaluate its commercial suitability. With this in mind, the aim of this research was to develop a thermodynamic model of V-groove double pass solar air collector and validate it through experimental results in terms of outlet air temperature, energy, and exergy efficiency. Performance and kinetics of the drying of apple in terms of moisture content, drying rate, specific energy consumption and exergy efficiency of dryer is studied. This is for the first time we have investigated the exergetic value of the energy in a V-groove double pass solar dyer demonstrating the inefficiencies and available work within the system. Techno-economic assessment of the process is fulfilled from the perspective of embodied energy and energy payback period.

2. Methodology

2.1. Experimental setup and procedure

This study investigates the thermal performance of double pass solar air heater for the application of drying in terms of first and second law efficiencies. ASHRAE Standard 93 requirements were followed that define the wind speed in the range of 2.2–4.5 m/s, maximum diffuse fraction to be 20 % and minimum solar irradiation to be 790 W/m^2 [58]. A pilot scale experimental set up located at the Queensland University of Technology in Brisbane (27.4705° S, 153.0260° E), Australia, was utilised as a case study. Apple, Pink Lady, was dried as a strategic fruit in Australia where 263,000 tonnes are produced annually [59]. From industrial perspective, quality, energy consumption and time management have been serious challenges [8]. Brisbane is considered to have high solar radiation where the solar irradiance is estimated to vary between 3 kWh/m^2/day in winter to more than 6 kWh/m^2/day in summer. The experimentation was performed in March 2022 from 09:00 am till 05:00 pm at similar ambient conditions with varying mass flow rates (0.021–0.061 kg/s). Experimental setup consisted of 3 main sections V-groove SAC, fan and drying chamber as shown in Fig. A.1and Fig. 1.

V-Groove SAC

A double pass solar air collector used for the experiment had the dimensions of 2x1 m (LxW) with a V-groove angle of 60° (Fig. A2) and consisted of a V-shaped aluminium absorber and a glass cover. Properties and dimensions of absorber and glass are given in Table 1.Two RTD sensors were installed (Fig. 1, RTD 3 and 4), one at the inlet and one at the outlet of solar air collector to measure the inlet and outlet temperature of air. Air leaving the solar air collector was passed to the drying chamber.

Drying chamber

A drying chamber was installed at the exit of solar air collector. The drying chamber was constructed out of 2.5 mm galvanized steel and consisted of three drying trays (30 % open area) insulated with glass cover and sealed with silicone to minimize the heat losses in the drying chamber. Two relative humidity and two RTD sensors (Fig. 1, RTD 5 and 6) were installed at the entrance and exit of drying chamber. One load cell was installed on the bottom of the drying chamber to measure the mass variation with respect to time.

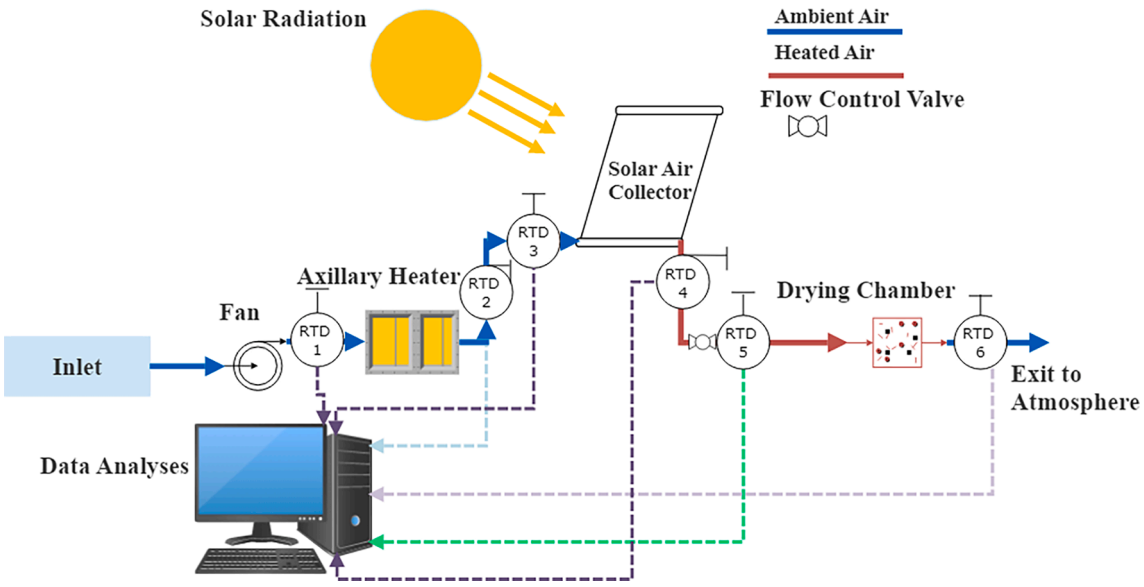

Fig. 1. Schematic of the experimental setup.

Table 1
Dimensional and material specification of solar dryer setup.

Parameters	Values	Units
V- Groove Absorber		
Length	2000	mm
Width	1000	mm
Thickness	1	mm
Emissivity (absorber)	0.05	
Absorptivity (absorber)	0.95	
Insulating material	Glass wool	
Rear and Side insulation	25	mm
Bottom insulation	50	mm
Glass Thickness	6 double glazed	mm
Drying Chamber		
Length	1003	mm
Width	315	mm
Height	270	mm
Drying Trays		
Length	602	mm
Width	252	mm
Thickness	1.5	mm
Hole Size	2	mm

Instrumentation

A pyranometer (Model TBQ-2-B) was used to measure the incoming solar radiation striking the SAC surface with field view of 180°. A load cell (Lorenze single point load cell type AG) was used to analyse the mass variation of the dried product with time. RTDs (GPD series from pyro-sales) were used to measure the temperature at inlet and exit of each part of the experimental setup. K-type (TC-TT-KI-24–2 M) was used to measure the bed temperature of thermal energy storage at various points. Anemometer-96792 was used to measure the air velocity at the inlet and outlet of solar air collector. Pasco (PS-2181) was used to measure the pressure drop in solar air collector.

Data collected from all the sensors was transferred to the relevant voltage/current national instrument (NI) module which is placed into the NI chassis. National instrument NI 9237 was used for thermocouples data, National instrument NI 9217 was used for RTDs data and National instruments NI 9208 was used for pressure and humidity data. All these three modules were connected to National instrument cDAQ-9188 chassis. Data from chassis was transmitted to data logging software LABVIEW through Ethernet.

2.2. Analysis

2.2.1. Mathematical modelling

A thermodynamic model of the system was developed in MATLAB and solved numerically. The system was assumed to be steady state and one-dimensional flow. Energy balance equations for the absorber plate, glass cover, air flow and back plate were developed based on heat transfer network, shown in Fig. 2, as.

$$\alpha_G I + (T_{F1} - T_G)h_{c,G-F} + (T_p - T_g)h_{r,P-G} = U_T(T_P - T_A) \quad (1)$$

$$h_{r,P-G}(T_P - T_G) + h_{c,P-F}(T_P - T_{F1}) + h_{r,P-B}(T_P - T_B) + h_{c,P-F}(T_P - T_{F2}) = \alpha_P \tau_G I \quad (2)$$

$$Q_1 + h_{c,G-F}(T_{F1} - T_G) = h_{c,P-F}(T_P - T_{F1}) \quad (3)$$

$$Q_2 + h_{c,B-F}(T_{F2} - T_B) = h_{c,P-F}(T_P - T_{F2}) \quad (4)$$

$$U_B(T_B - T_A) = h_{c,B-F}(T_{F2} - T_B) + h_{r,P-B}(T_P - T_B) \quad (5)$$

where α is the absorptivity, T is the temperature (°C), h is heat transfer coefficient (W/m^2 °C), U is the heat loss coefficient (W/m^2 °C), τ is the transmissivity and I is the solar irradiance (W/m^2). The subscripts, G, P, B, A, r, c, F_1 and F_2 represent glass, absorber plate, back plate, ambient, radiative, convective, fluid pass above the absorber plate, and fluid pass below the absorber plate, respectively.

To analyse the performance of solar air collector, heat transfer co-efficients and losses need to be evaluated. Radiation heat transfer co-efficients can be determined using the following equations:

Radiation heat transfer coefficient between ambient and glass cover [60]:

$$h_{r,G-A} = \sigma \varepsilon_G (T_G - T_A)(T_G^2 - T_A^2) \quad (6)$$

where σ and ε are Stefan Boltzmann constant (5.67x10^{-8} W/m^{2}K^4) and emissivity.

Radiation heat transfer coefficient between the plate and glass cover, plate and back plate [60]:

$$h_{r,P-G} = \frac{\sigma(T_P + T_G)(T_P^2 + T_G^2)}{\left(\frac{1}{\varepsilon_P}\right) + \left(\frac{1}{\varepsilon_G}\right) - 1} \quad (7)$$

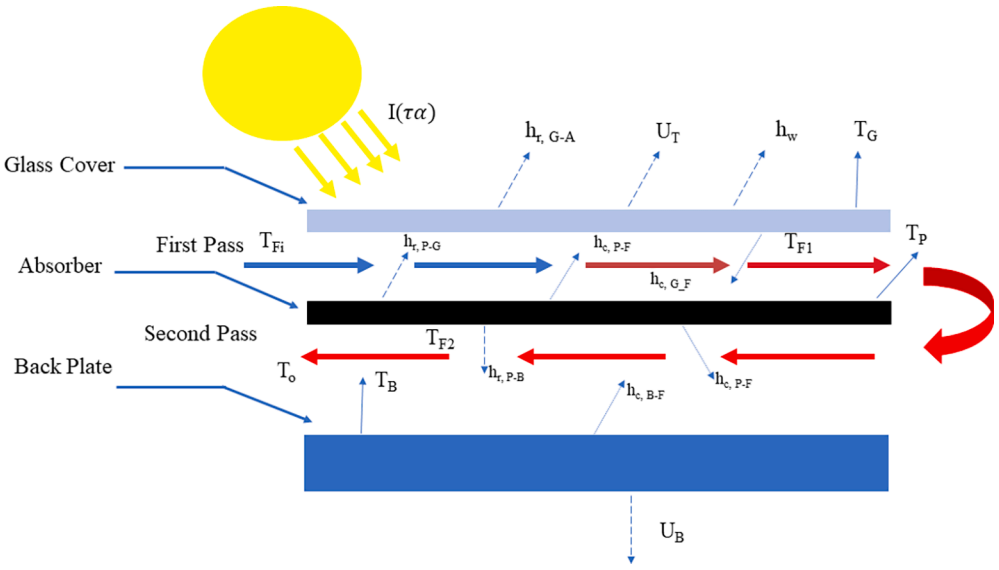

Fig. 2. Illustration of heat transfer coefficients in the elements of the SAC.

$$h_{r,P-B} = \frac{\sigma(T_P + T_B)\left(T_P^2 + T_B^2\right)}{\left(\frac{1}{\varepsilon_P}\right) + \left(\frac{1}{\varepsilon_B}\right) - 1} \tag{8}$$

Overall heat loss coefficient was determined by using the following equation [61]:

$$U_L = U_T + U_B + U_E \tag{9}$$

where U_T is the top loss coefficient and was evaluated using the following equation [61]:

$$U_T = \left(\frac{N_G}{\frac{X}{T_P}\left[\frac{T_P - T_A}{N_G + Y}\right]^{0.33} + \frac{1}{h_w}}\right)^{-1} + \frac{\sigma(T_P - T_A)\left(T_P^2 - T_A^2\right)}{\left(\frac{1}{\varepsilon_P + 0.05N_G(1-\varepsilon_P)}\right) + \left(\frac{(2N_G + Y - 1)}{\varepsilon_P}\right) - 1} \tag{10}$$

where N_G is the number of glass covers, X and Y are coefficients determined by the following equations [61]:

$$X = 365.9\left(1 - 0.0083\beta + 0.0001298\beta^2\right) \tag{11}$$

$$Y = \left(1 - 0.04h_w + 0.0005h_w^2\right)(1 + 0.091N_G) \tag{12}$$

where h_w is the wind heat transfer coefficient and is given as,

$$h_w = 5.7 + 3.8V \tag{13}$$

where V is the mean ambient air velocity.

In Eq. (9), U_B is the bottom heat loss coefficient:

$$U_B = \frac{1}{\frac{x}{k_i} + \frac{1}{h_w}} \tag{14}$$

x and k_i are insulation thickness (m) and thermal conductivity (W/mK), respectively. Convective heat transfer coefficient for the fluid passing through the first pass was evaluated using the following equations [62] assuming that:

$$h_{c,G-F} = h_{c,P-F1} \tag{15}$$

$$h_{c,G-F} = \frac{Nu_1 k}{D_h} \tag{16}$$

However, absorber plate used is the V-groove so area of the bottom channels is less than the developed are of the plate by $\frac{1}{\sin\frac{\theta}{2}}$ factor, thus the new value of $h_{c,G-F}$ is given as [63],

$$h_{c,G-F} = \frac{Nu_1 k}{D_h}\frac{1}{\sin\left(\frac{\theta}{2}\right)} \tag{17}$$

where θ is the induced v-groove angle, D_h is the hydraulic diameter of the duct,

$$D_{h1} = H_{collector} + \frac{H_{groove}}{2} \tag{18}$$

where D_h is the hydraulic diameter (m), H is the height of collector and groove, respectively (m).

If flow is laminar (Re less than 2800).

$$Nu = 2.821 + 0.126Re\frac{H_{groove}}{L} \tag{19}$$

If flow is transient ($2800 < \mathrm{Re} < 10^4$).

$$Nu = 1.9 \times 10^{-6}Re^{1.79} + 225\frac{H_{groove}}{L} \tag{20}$$

If flow is turbulent ($10^4 < \mathrm{Re}$).

$$Nu = 0.0302Re^{0.74} + 0.242Re^{0.74}\frac{H_{groove}}{L} \tag{21}$$

Convective heat transfer coefficient for second pass with the assumption that:

$$h_{c,P-F2} = h_{c.B-F2} \tag{22}$$

$$h_{c,P-F2} = \frac{Nu_2 k}{D_{h2}} \tag{23}$$

D_{h2} is the hydraulic diameter of air flow for second pass which was equal to the $\frac{2}{3}H_{groove}$. Heat transferred to air during first and second pass was evaluated using:

For first pass

$$Q_1 = \dot{m}C_p(T_{F1} - T_{Fi}) \tag{24}$$

Q_1 represents the amount of heat transferred to the air (Watt) flowing through the first pass of the absorber.

For the second pass

$$Q_2 = \dot{m}C_p(T_{F2} - T_{F1}) \tag{25}$$

while Q_2 is the amount of heat transferred (Watt) to the air flowing through the second pass of the absorber. where C_p is the specific heat constant (J/kgK) and $\dot{m}$ is the mass flow rate of air (kg/s).

After evaluating heat transfer to air, radiative and convective heat transfer coefficient and overall heat loss coefficients, outlet air temperature of solar air collector was determined using the following equation:

$$T_o = T_{Fi} + \frac{Q_1 + Q_2}{\dot{m}C_p} \tag{26}$$

Eq (1)-(5) were rearranged into the following equations for matrix evaluation to analyse the outlet air temperature of air:

$$\alpha_G I + U_T T_A = \left(h_{c,G-F} + h_{r,P-G} + U_T\right)T_G - h_{c,G-F}T_{F1} - h_{r,P-G}T_P \tag{27}$$

$$-h_{r,P-G}T_G - h_{c,P-F1}T_F + \left(h_{c,P-F} + h_{c,P-F2} + h_{r,P-B} + h_{r,P-G}\right)T_P - h_{c,P-F2}T_{F2} - h_{r,P-B}T_B = \alpha_P \tau_G I \tag{28}$$

$$h_{c,G-F1}T_G - \left(h_{c,G-F1} + h_{c,P-F1} + \dot{m}C_p\right)T_{F1} + h_{c,P-F1}T_P = \dot{m}C_p T_{Fi} \tag{29}$$

$$\dot{m}C_p T_{F1} + h_{c,P-F2}T_P - \left(h_{c,P-F2} + h_{c,B-F2} + \dot{m}C_p\right)T_{F2} + h_{c,B-F2}T_B = 0 \tag{30}$$

$$-h_{r,P-B}T_P - h_{c,B-F2}T_{F2} + \left(h_{r,P-B} + U_B + h_{c,B-F2}\right)T_B = U_B T_A \tag{31}$$

Eq. 27–31 were arranged into 5x5 matrix in the form:

$$[A][T] = [B] \tag{32}$$

Calculated temperatures will be compared to the previous temperature values. The process was repeated until all the temperature difference between previous and newly measured temperatures was less than 0.01 °C.

Thermal efficiency

Thermal efficiency of SAC was calculated using the Eq. (33).

$$\eta = \frac{\dot{m}C_p(T_o - T_{Fi})}{IA} \tag{33}$$

2.2.2. Exergy analysis

Exergy is indication of useful energy available to the system. It provides information on the irreversibility and optimisation potentials of the processes. Exergy balance for a steady state process is as follow:

$$\sum \dot{Ex}_i - \sum \dot{Ex}_o = \sum \dot{Ex}_{dest} \tag{34}$$

Or

$$\sum\left(1 - \frac{T_e}{T_s}\right)\dot{Q}_s - \dot{W} + \sum \dot{m}_i\psi_i - \sum \dot{m}_o\psi_o = \dot{Ex}_{dest} \tag{35}$$

where ψ is the specific exergy (kJ/kg) and Ex_{dest} is the exergy destruction. The subscripts e and s represent the environment and sun temperature.

$$\psi_i = (h_i - h_e) - T_e(s_i - s_e) \tag{36}$$

$$\psi_o = (h_o - h_e) - T_e(s_o - s_e) \tag{37}$$

where h and s are the enthalpy (J) and entropy generation (J/K). substituting Eqs. (36) and (37) into Eq. (35) yields:

$$\sum\left(1 - \frac{T_e}{T_s}\right)\dot{Q}_s - \dot{m}[(h_o - h_i) - T_e(s_o - s_i)] = \dot{Ex}_{dest} \tag{38}$$

where $\dot{Q}_s$ is the absorbed solar irradiation and is given by:

$$\dot{Q}_s = I\tau\alpha A_c \tag{39}$$

change in enthalpy and entropy within SAC is given as:

$$\Delta h = h_o - h_i = C_p(T_o - T_i) \tag{40}$$

$$\Delta s = s_o - s_i = C_p\left(\ln\left(\frac{T_o}{T_i}\right) - Rln\left(\frac{P_o}{P_i}\right)\right) \tag{41}$$

Exergy efficiency of solar air collector was evaluated using Eq. (42):

$$\eta_{II} = \frac{Ex_o}{Ex_i} = 1 - \left(\frac{Ex_{dest}}{\left(1 - \left(\frac{T_e}{T_s}\right)\right)\dot{Q}_s}\right) \tag{42}$$

Sustainability Index and Improvement Potential

Sustainability index and improvement potential are the major parameters of the exergy sustainability indicator that assist in identifying how exergy losses affect the system sustainability and how much a system can further improve.

$$SI = \frac{1}{1 - \eta_{II}} \tag{43}$$

$$IP = (1 - \eta_{II})(Ex_i - Ex_o) \tag{44}$$

2.2.3. Drying analysis

Drying involves the removal of moisture from the desired product up to allowable limits. In this study, pink lady apples with the initial

moisture content of 81.8 % were sliced to 4.2 mm thickness. Moisture ratio was calculated using the following equation:

$$M.R = \frac{M_t - M_e}{M_o - M_e} \tag{45}$$

where M_t, M_e and M_o are moisture content at any time t, equilibrium moisture content and initial moisture content at t = 0 *sec* on wet basis (%), respectively. Eq. (45) can be shortened to Eq. (46), as M_e can be assumed to be negligible [42]:

$$M.R = \frac{M_t}{M_o} \tag{46}$$

Drying rate is a crucial parameter in drying analyses which gives the amount of moisture evaporated over time [64]:

$$DR = \frac{M_o - M_f}{\Delta t} \tag{47}$$

Exergy Analysis of Dryer

Exergy equations for solar drying chamber is given by:

$$\sum \dot{Ex}_{dest,DC} = \sum \dot{Ex}_{i,DC} - \sum \dot{Ex}_{o,DC} \tag{48}$$

Inlet exergy of drying air is:

$$Ex_{i,DC} = m_a C_p \left[\left(T_{i,DC} - T_A\right) - T_A \ln\left(\frac{T_{i,DC}}{T_A}\right) \right] \tag{49}$$

Exergy out of drying air:

$$Ex_{o,DC} = m_a C_p \left[\left(T_{o,DC} - T_A\right) - T_A \ln\left(\frac{T_{o,DC}}{T_A}\right) \right] \tag{50}$$

$$\eta_{dryerexergy} = \frac{Ex_{o,DC}}{Ex_{i,DC}} \tag{51}$$

2.2.4. Techno-Economic analysis (TEA)

A generic techno-economic analysis examines costs, benefits, risks, uncertainties, and timeframes to evaluate the attributes of energy technologies. Manufacturing costs can be broken down into two main categories: capital expenses and operating expenses. Capital expenses are non-recurring costs such as equipment, buildings, and construction. In a TEA, these one-time facility costs are amortized over the assets' useful lifetime to relate capital expenses to a specific production volume. Operating expenses are recurring costs such as materials, labour, and energy. In this research, energy payback time (EPBT), energy yield factor and specific energy consumption (*SEC*) of a solar drying system are calculated as major measures of TEA. Eq. (52) was used to calculate Energy Payback Time:

$$EPBT = \frac{embodiedenergy}{annualusefulenergy} \tag{52}$$

Embodied energy is a calculation of all the energy that is used to produce a material or product, including mining, manufacture, and transport. International standards have been developed for calculating the embodied energy of products (for example, ISO 14067:2018 Greenhouse gases – Carbon footprint of products – Requirements and guidelines for quantification). The calculation of embodied energy is often performed within a lifecycle assessment (LCA) framework (ISO 14040:2006 Environmental management — Life cycle assessment — Principles and framework). A measure to understand how renewable energy can be best configured and operated to maximize the amount of heat the system will generate over the course of its service lifetime while minimizing costs, is energy yield factor calculated as Eq. (53):

$$Energyyieldfactor = \frac{totalcalculatedcostofthesystem}{usefullifetime} \tag{53}$$

Energy yield is the actual amount of energy harvested, taking into consideration external factors like heat, dirt, and shade, whereas efficiency refers simply to testing done in lab conditions.

Table 2
Errors and uncertainties of instrumentation and drying parameters.

Instrument	Error
Pyranometer	±2%
Resistance thermometer detector (RTD)	±3%
K-Type Thermocouples	±2.2 °C or 2 %
Load Cell	±0.017%
Humidity Sensor	±2%
Anemometer	±3%
Parameters	**Uncertainty**
Air Temperature	±0.94%
Thermal Efficiency	±2.68%
Exergy Efficiency	±1.37%
Dryer Exergy Efficiency	±1.37%
Moisture content	±0.99%

Amount of energy to remove moisture from fruits is formulated by specific energy consumption (*SEC*) [65]. To calculate *SEC*, several electrical devices including fan and instrumentation were monitored and their power consumption was measured at the varying mass flow rates Eq. (54):

$$SEC = \frac{E_{electricity}}{m_w} \tag{54}$$

where m_w is mass of evaporated water [66]:

$$m_w = \frac{(M_0 - M_f)}{100 - M_f} \times W_o \tag{55}$$

where M_0 and M_f are the initial and final moisture content on wet basis (%), respectively and W_o is the mass of product (kg) at t = 0 *sec*.

2.2.5. Uncertainty analysis

Uncertainty analysis was performed on thermal performance of the system (temperature, energy, and exergy efficiency). The method described by [67] was used to evaluate the uncertainty for the current study. It involves a dependent function R and independent variables such as $v_1, v_2, v_3 \cdots . v_n$. Thus,

$$R = f(v_1, v_2, v_3 \cdots, v_n) \tag{56}$$

Uncertainty of R can be calculated as:

$$\delta R = \sqrt{\left(\frac{\delta R}{\delta v_1}\delta v_1\right)^2 + \left(\frac{\delta R}{\delta v_2}\delta v_2\right)^2 + \cdots + \left(\frac{\delta R}{\delta v_n}\delta v_n\right)^2} \tag{57}$$

where δR is the uncertainty in the function R, $\frac{\delta R}{\delta v_n}$ is the partial derivative of R with corresponding v_i. δv_i is the uncertainty in the parameter. Uncertainty values for instruments and parameters are given in Table 2.

2.3. Framework methodology

A hierarchy of the study can be seen in Fig. 3 The methodology based on developing a thermodynamic model using the real time solar radiation measured by the pyranometer installed at the setup and mass flow rate (0.021–0.061 kg/s) in Brisbane, Australia. Outputs from the model were compared with experimental results to be validated.

3. Result and discussion

Results are divided into three sections. Firstly, thermodynamic model and experimental results were compared in terms of outlet air temperature, energy, and exergy efficiency. In second section, experimental results were compared at different flow rates (0.021–0.061 kg/s) for solar air collector. At last, drying kinetics of apple was discussed with economic analysis in terms of energy payback period based on specific

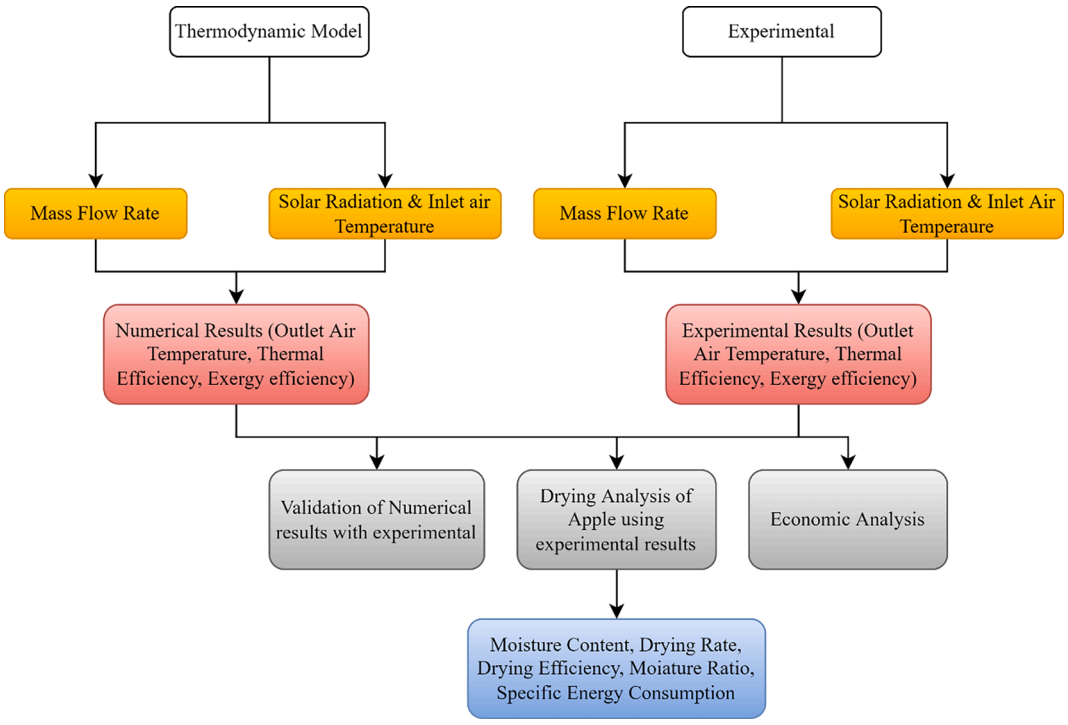

Fig. 3. Hierarchy of the study.

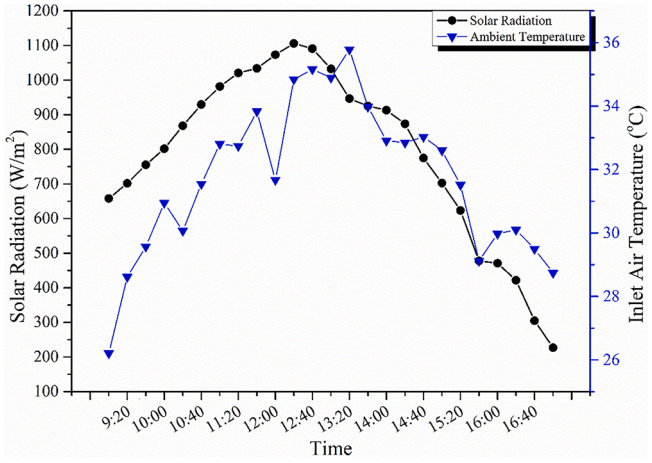

Fig. 4. Variation of solar radiation and ambient temperature with time.

Table 3
RMSE of outlet air temperature, thermal efficiency, and exergy efficiency.

Flow Rate (kg/s)	RMSE Outlet Temperature	RMSE Thermal Efficiency	RMSE Exergy Efficiency
0.021	5.53	11.56	1.22
0.031	5.20	9.30	1.04
0.041	4.90	9.07	0.95
0.051	4.46	8.30	0.89
0.061	3.87	7.70	0.84

energy consumption.

3.1. Solar radiation

Experiments were conducted in March-April 2022, in the city of Brisbane, Australia. Average wind speed and mean ambient temperature were acquired from the Queensland University of Technology's metrological module to be 1.58 m/s and 33.2 °C, respectively. Fig. 4 shows the variation of solar radiation with daytime. Maximum solar radiation achieved was 1105.92 W/m^2 around 12:00 pm.

3.2. Numerical validation

3.2.1. Outlet air temperature

Figure 5 (a-e) represents the comparison of predicted and experimental outlet air temperature for the V-groove double pass solar air collector. The trend is analogous for the predicted and experimental values in the sense that increasing mass flow rate leads to a reduction in the outlet air temperature. Also, it is observed that the outlet air temperature is strongly related to solar radiation as the heat transfer rate between the absorber and air increases with solar radiation. Maximum outlet air temperatures achieved for numerical and experimental investigations were 84.95 °C and 81.03 °C, respectively, at the mass flow rate of 0.021 kg/s. Sun et al. [16] numerically achieved outlet air temperature of 72 °C at 0.020 kg/s in a flat plate air collector. Daliran et al. [68] numerically and experimental achieved the outlet air temperature of 83 °C and 74 °C, respectively, using solar air collector integrated with fins.

Higher deviations at the initial hours of the experimentation correspond to unsteady conditions of the set up and mitigate as the system is stabled.

The thermodynamic model underpredicted the outlet air temperature during the peak hours at 0.061 kg/s flow rate compared to experimental results. Table 3 represents the root mean square error (RMSE) of predicting outlet air temperature. The residence time of air increases in the collector at low mass flow rate allowing air temperature to increase significantly at the expense of high heat losses which resulted maximum RMSE of 5.53 °C at lowest mass flow rate. Fig. 5 and Table 3 also show that an increase in mass flow rate caused the decrement in outlet air temperature but, this also reduced the RMSE between mathematical model and experimental setup. Additionally, at high flow rates, the thermodynamic model predicted the experimental results better.

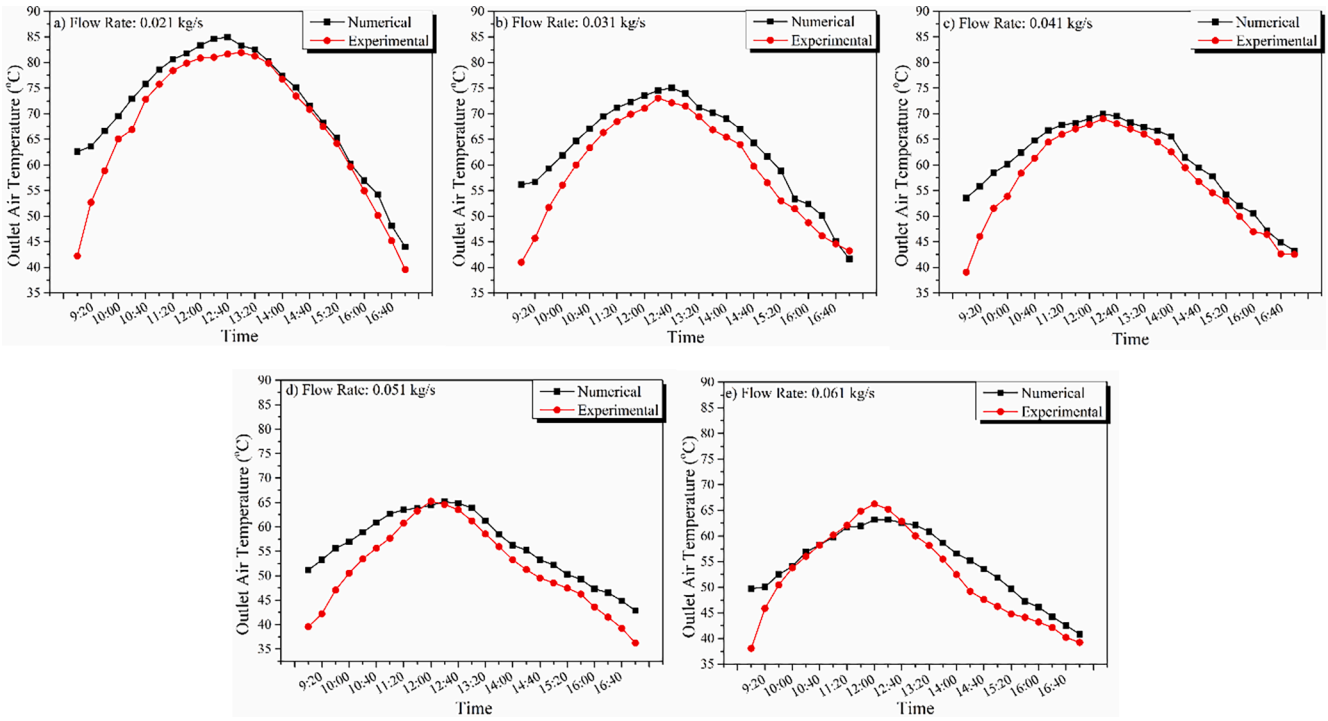

Fig. 5. Comparison of simulated and experimental outlet air temperatures at different flow rates a) 0.021 kg/s b) 0.031 kg/s c) 0.041 kg/s d) 0.051 kg/s e) 0.061 kg/s.

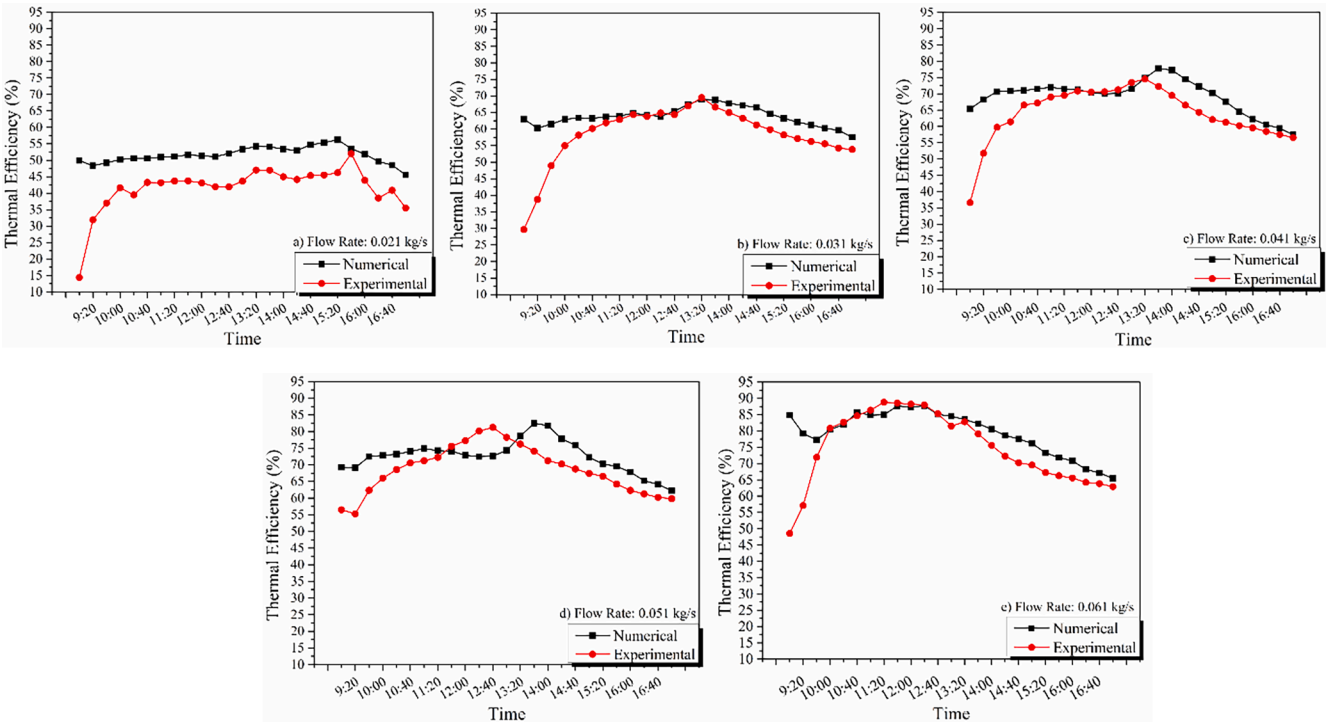

Fig. 6. Comparison of model prediction and experimental thermal efficiency at different flow rates a) 0.021 kg/s b) 0.031 kg/s c) 0.041 kg/s d) 0.051 kg/s e) 0.061 kg/s.

3.2.2. Thermal efficiency

The thermal efficiency of the solar air heater was evaluated considering the outlet air temperature and solar radiation for the thermodynamic model. Additionally, the results were then compared with the experimental results as shown in Fig. 6 (a-e). For the mass flow rate of 0.061 kg/s, maximum thermal efficiencies achieved were 87.6 % and 88.50 % for the thermodynamic and experimental approaches, respectively. Comparison of numerical and experimental thermal efficiency in solar air collectors has been reported in the literature, Sun et al. [16] numerically achieved thermal efficiency of 55 % using flat plate solar air collector at 0.050 kg/s flow rate. The same value was reported by Daliran et al. [68] who theoretically evaluated the thermal efficiency of

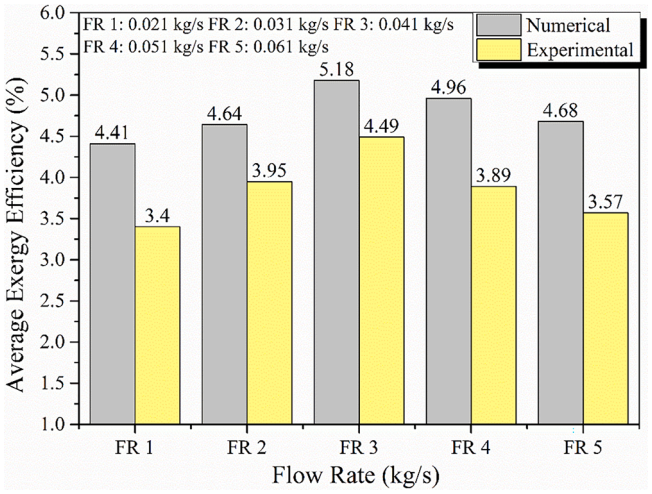

Fig. 7. Mathematical and experimental average exergy efficiency of solar air collector at different mass flow rates.

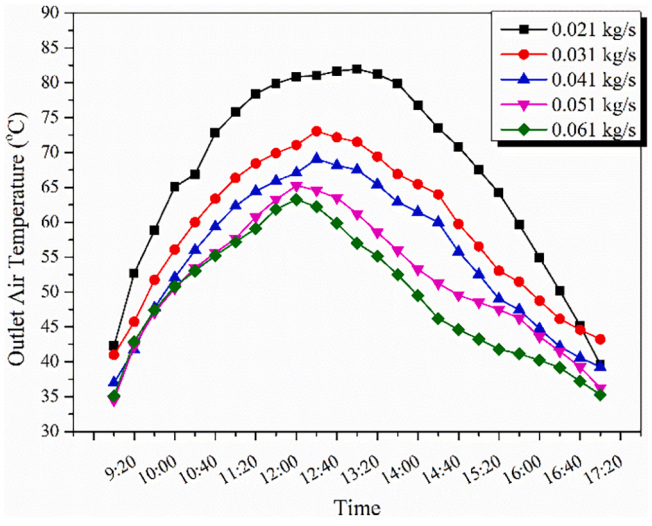

Fig. 8. Variation of experimental outlet air temperature with respect to time and mass flow rate.

solar air heater with fins. The thermal efficiency increased with the mass flow rate which was observed in both the thermodynamic model and the experimentations. However, the significant difference was observed between the thermodynamic and experimental thermal efficiency at the start of the experiment. This was due to the unsteady state of experimental setup in the beginning of experiments. Thus, RMSE of thermal efficiency was higher which might be reduced by assuming steady state for the experimental setup.

RMSE between predicted and actual thermal efficiency at different flow rates can be seen in Table 3. Since thermal efficiency is proportional to temperature difference, any reduction of error in temperature resulting from higher mass flow rates can contribute to reduced error in thermal efficiency. That may be the main reason for smaller RMSE at high mass flow rates.

3.2.3. Exergy efficiency

Exergy efficiency is highly dependent on outlet air temperature and mass flow rate. A comparison of the thermodynamic and experimentally evaluated average exergy efficiency at different flow rates with associated RMSE can be seen in Fig. 7. Exergy efficiency was enhanced by raising the mass flow rate up to an optimum mass flow rate with maximum RMSE of 1.22 %, Table 3. This was observed in both the model and the experimentation. Above the optimum mass flow rate, outlet air temperature starts to dominate rather than the mass flow rate. Outlet air temperature reduces with increments in mass flow rate resulted in a decrement in exergy efficiency at higher mass flow rates. At mass flow rate of 0.041 kg/s, the average exergy efficiency was evaluated to be 5.18 % and 4.49 % theoretically and experimentally, respectively. While the maximum theoretical exergy efficiency at 0.051 kg/s flow rate was 6.56 % which is comparable to Matheswaran et al. [69] who achieved a exergy efficiency of 4.36 % for single pass double jet plate solar collector.

3.3. Solar air collector performance

3.3.1. Outlet air temperature

Fig. 8 represents the effect of five different flow rates (0.021, 0.031, 0.041, 0.051 and 0.061 kg/s) on the experimentally measured outlet air temperature with respect to daytime from 09:00 AM to 05:00 pm. As already discussed before, air temperature follows closely the solar radiation and peaked at 12:00 pm (peak solar radiation) and dropped when the radiation decreased on the surface. Maximum outlet air temperature was 81.96 °C, 73.06 °C, 69.06 °C, 65.25 °C, and 62.21 °C for 0.021 kg/s, 0.031 kg/s, 0.041 kg/s, 0.051 kg/s and 0.061 kg/s, respectively. The main reason for reduced air temperature with the flow rate is low residence time of air within the air heater. This result is regarded as a desirable performance of the collector comparing with 80.5 °C for natural convection and 49 °C for forced convection (0.032 kg/s flow rate) as reported by Salih et al. [31] on a V-groove absorber with porous media. Karim et al. [70] achieved maximum outlet air temperature of 62.9 °C at 0.011 kg/s flow rate using V-groove absorber. Daliran et al. [68] gained the outlet air temperature of 64.64 °C at 0.033 kg/s using longitudinal fins. Comparing outlet air temperature with the literature shows a significant difference representing the effectiveness of the V-groove double pass absorber.

3.3.2. Thermal efficiency

The variation of experimental thermal efficiency with flow rate and solar radiation can be found in Fig. 9. Three zones increasing, constant and falling was observed in thermal efficiency with respect to time. At the start of the day, thermal efficiency variation complies with solar radiation, while after 12:00 pm, the trend is constant up to 3 pm. Due to energy stored in the V-groove double pass absorber, thermal efficiency does not follow the decreasing trend like radiation. From Fig. 9, it can be deduced that mass flow rate has a positive impact on thermal efficiency,

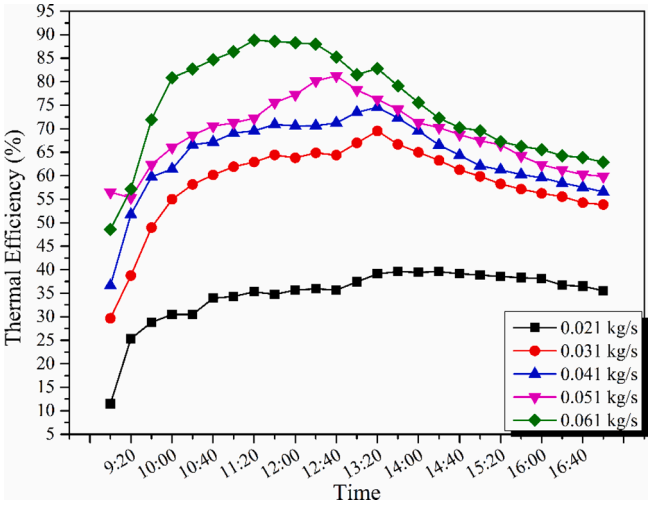

Fig. 9. Variation of experimental thermal efficiency with respect to time and mass flow rates.

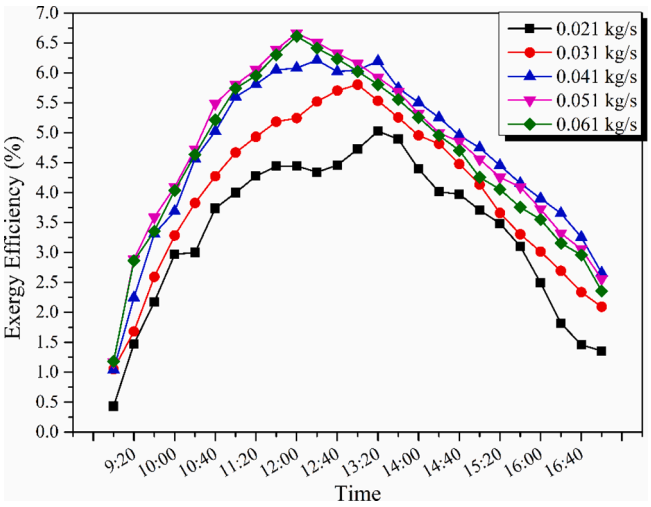

Fig. 10. Variation of experimental exergy efficiency with respect to time and mass flow rate.

despite the reduction in the outlet temperature. Surface roughness of the v-groove plate plays a critical role in enhancing the thermal efficiency of solar air collector by enhancing heat transfer to the air. Maximum thermal efficiency was observed to be 88.8 % at 0.061 kg/s which is comparable to the thermal efficiency of flat plate solar air collectors [32].

3.3.3. Exergy efficiency

The experimental exergy efficiency variation with respect to mass flow rate and time can be seen in Fig. 10. Exergy efficiency is mainly dependent on three variables: mass flow rate, outlet air temperature and solar radiation. From Fig. 10, exergy efficiency followed the trend with respect to solar radiation as compared to the outlet air temperature. This is because as exergy efficiency is a function of outlet air temperature and outlet air temperature is highly dependent on solar radiation. As soon as the solar radiation starts to drop, outlet air temperature decreases causing the enthalpy of the system to decrease which had a negative impact on exergy efficiency.

Maximum exergy efficiency achieved was 6.66 % at 0.051 kg/s which is more than exergy efficiency of flat plate double pass solar air heater and zig-zag copper tube solar air heater which was 3.5 % and 5.84 % achieved by Abo-Elfadl et al. [32] and Kumar et al. [45]. Average exergy efficiency increases with increase in mass flow rate up to an optimum level of 0.041 kg/s. Exergy efficiency at 0.051 and 0.061 kg/s drops below the efficiency at 0.041 kg/s after the 12:00 pm due to reduced outlet air temperature at higher mass flow rates. Maximum average daily exergy efficiency was 4.49 % at 0.041 kg/s.

The low values of exergy efficiency in solar dryers proves that a great deal of irreversibility exists in the system. The source of such irreversibility can be mixings in flow streams, duct section changes and heat transfer. This exergetic investigation provides a more precise understanding of energy in the system, i.e. the quality of energy that the system is harnessing, rather than accounting quantity of energy utilised.

3.4. Drying analysis of apple

3.4.1. Moisture content and drying rate

Samples were dried from 09:00 am to 05:00 pm (Fig. 11) at the flow rates of 0.021, 0.031, 0.041, 0.051 and 0.061 kg/s. The corresponding final moisture content (wet basis) was 19.89 %, 16.02 %, 13.11 %, 15.85 %, and 15.95 %, respectively.

Drying kinetics is plotted in Fig. 12. As predicted, increase in the mass flow rate up to an optimum point, enhances the moisture removal rate from the apple as shown in Fig. 12a and 12b. Lower air temperature and reduced contact time of air with the product occur at higher mass flow leading to reduced moisture removal and drying rate. Experimentation performed by Das et al. [71] using indirect solar dryer corroborated the similar trend. From Fig. 12a Fig. 12b, the optimum mass flow rate was 0.041 kg/s. Akbulut et al. [72] found that change in moisture content was high for the mass flow rate of 0.036 kg/s compared to 0.014 kg/s, 0.02 kg/s and 0.033 kg/s in the indirect solar drying of mulberry.

Fig. 12b illustrates the effect of mass flow rate on the drying rate of apple. Drying rate increases at the start for all flow rates due to high free moisture in the product and faster mass transfer. After 90 min, drying rate started to decrease for all mass flow rates. From 90 to 250 min, slope of drying rate at mass flow rate 0.031, 0.041, 0.051 and 0.061 kg/s was very steep because of high moisture content at the surface of apple slices, as soon as the surface moisture decreases, a thin layer of gel formed at the product surface which do not allow more moisture to be removed and required high energy to mitigate the remaining moisture content [42]. That is why, drying rate at flow rate 0.021 kg/s was high after 200 min compared to other mass flow rates due to the dominant effect of temperature instead of flow rate on the drying rate.

3.4.2. Dryer exergy analysis

3.4.2.1. Exergy efficiency. Fig. 13 shows the exergy efficiency of dryer with respect to mass flow rate and time. Exergy efficiency of dryer increases with drying time and mass flow rate. Mugi et al. [73], Akbulut and Durmus et al. [72] and Vijayan et al. [74] had the similar result of dryer exergy efficiency with respect to time and mass flow rate.

3.4.3. Techno-economic view

Specific energy consumption (*SEC*) is a vital indicator for analysing the system effectiveness compared to the conventional dryer. Annual non-renewable energy consumption of the system is obtained to be 576 kWh and 817.92 kWh for mass flow rates of 0.021 kg/s and 0.061 kg/s, respectively. These values were used in estimating *SEC*. The corresponding SECs for the mentioned flow rates will be 3.09 kWh/kg and 4.39 kWh/kg. Fig. 14 compares *SEC* in two scenarios: first, the current experimental dryer which benefits SAC as a renewable solar energy to dry the samples, and second, when all the energy should be provided by electricity. As observed, *SEC* increases with flow rates which is predictable. But 53.8 % reduction of *SEC* is obtained by solar sourcing of the

Fig. 11. Dried pink lady apple using solar air heater.

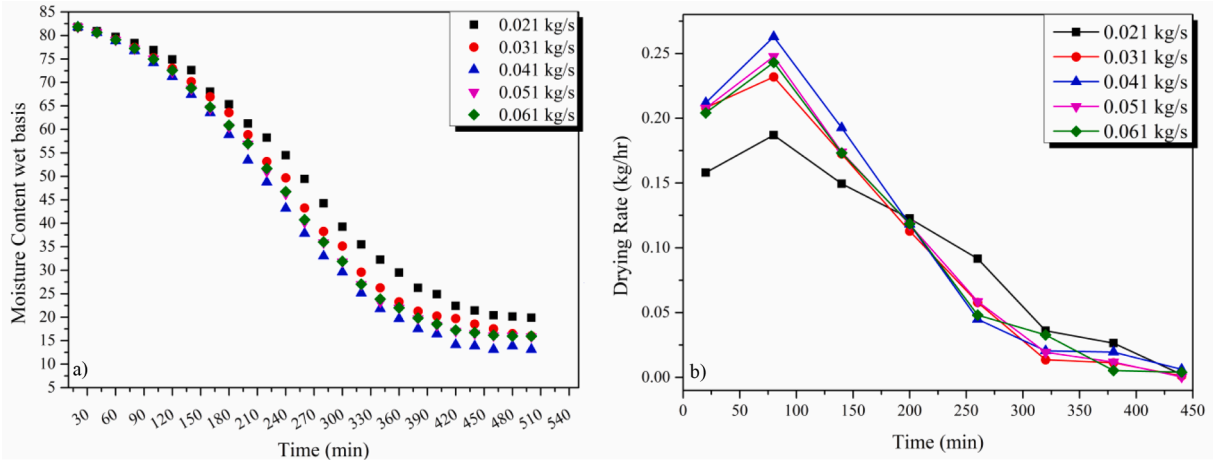

Fig. 12. Effect of mass flow rate on a) moisture content and b) drying rate.

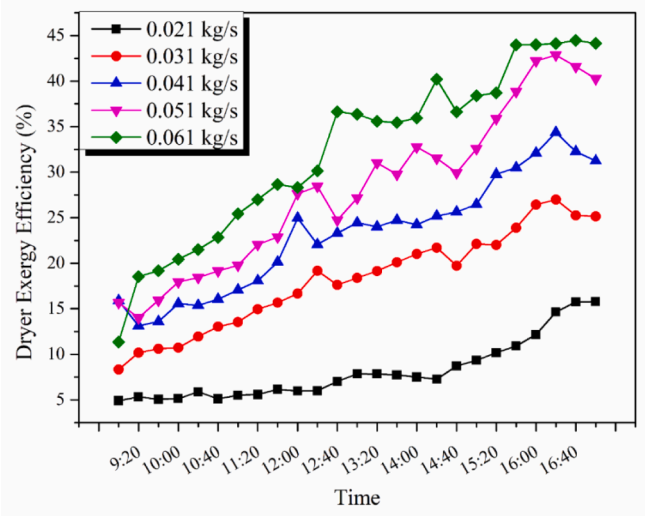

Fig. 13. Variation of dryer exergy efficiency with respect to time and mass flow rates.

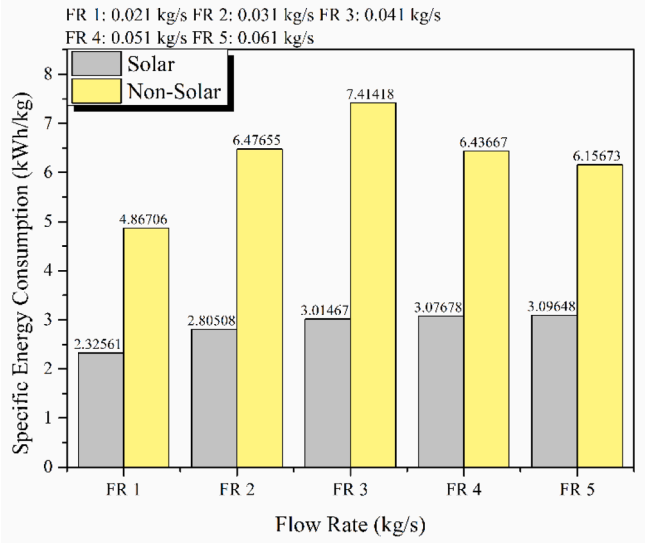

Fig. 14. Specific energy consumption for solar and non solar scenario.

Table 4
Embodied energy of components of the solar dryer [74,77,78].

Component	Materials	Energy Density (kWh/kg)	Mass of Component (kg)	Embodied Energy (kWh)
V-groove Plate	Aluminium	55.28	11	608.08
Glass cover	Glass	7.28	3	21.84
Blower	–	19.5	5	97.5
Ducts and Frames	Mild Steel	8.89	60	533.4
PVC piping	PVC	22	10	220
Insulation	Fibre Glass wool	4.044	4.5	18.2
Coatings	Grey and black paint	25.11	0.5	12.55
drying Chamber	Steel	8.89	10	88.9
Instrumentation and panel	–	–	–	33
Total				**1633.47**

dryer energy demand which shows the benefit of using solar dryer. By considering the average electricity tariff in Queensland, Australia to be 0.18 USD/kWh [75] and 250 days of drying annually, this is equivalent to 222.51 USD per 1 kg of apple when electricity is applied, and 90.39 USD per 1 kg of apple when solar air heater is used. In the other words, 59 % reduction in electricity tariffs is achieved.

Total energy embodied for the solar dryer setup was calculated for solar collector, installations, maintenance, joints and fittings, instrumentations, fan and chambers. The calculation of embodied energy is often performed within a lifecycle assessment (LCA) framework developed by ISO 14040:2006, Environmental management, Life cycle assessment- Principles and framework [76]. Table 4 has detailed the components and corresponding embodied energies:

Total embodied energy (EE) of the combined solar system and the dryer is calculated to be 1633.47 kWh. Gupta et al. [56] calculated the embodied energy of a photovoltaic-thermal solar dryer to be 3124 kWh. The major contribution in EE is the PV module and mild steel [56]. This is also corroborated by Ardente et al. [79] for a thermal solar collector and Mugi et al. [80] for a solar dryer for drying of guava slices. The major components sharing the most EE in the production of double pass V-groove solar dryer are aluminum and steel with EE of 608.08 kWh as given in Table 4. To optimize the facility from the perspective of life cycle energy, application of copper with the EE of 19.61 kWh/kg is proposed for the absorber plate. To have a practical measure of the life cycle energy performance of the system, energy payback Time (EPBT) was calculated from Equation (52). Annual useful energy of the dryer was estimated by calculating average solar absorption in the collector throughout the year. The data from Kelvin Grove station of QUT,

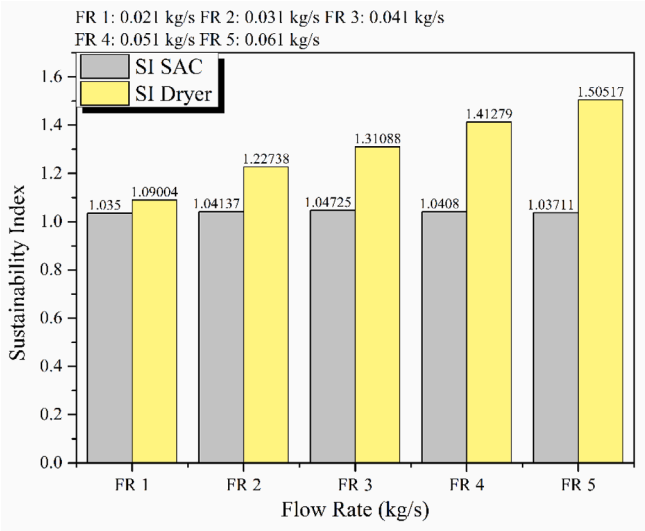

Fig. 15. Sustainability index of the system for different mass flow rates.

Brisbane were adopted for solar radiation in time series in 2019 as a sample year. Utilized energy obtained from the collector was measured to be 2080.32 kWh for 8 h of working between 9 am and 5 pm of Brisbane, Australia. EPBT was calculated to be 0.78 years which is much lower than the lifetime of the system and clearly expresses that the system is justified when energetic view is pinpointed. In the other words, the system is capable to deliver energy for a larger scale application. Total cost of the system in 2012, manufacturing date, was 17,240 AUD (Australian dollars), which was converted to the future value of 2022 with the interest rate of 6 % to be 30,874 AUD. Therefore, Energy Yield Factor was calculated to be 1235 from Equation (53).

3.5. Sustainability index and improvement potential

Fig. 15 represent the sustainability of the system for solar air collector and dryer. Minor increase in sustainability index of solar air collector was noticed with respect to mass flow rate while dryer sustainability index was substantially increased with increase in mass flow rate. As sustainability index is the function of exergy efficiency, therefore the exergy efficiency of solar air collector was affected by the mass flow rate causing the sustainability index not to increase significantly with flow rate. While exergy efficiency of dryer was raised with mass flow rate allowing sustainability of the system to increase significantly. Maximum sustainability index achieved was 1.047 for SAC at 0.041 kg/s and 1.50517 for dryer at 0.061 kg/s, respectively.

Improvement potential is the indicator that how much a system has the potential to improve. Fig. 16 shows the improvement potential of solar air collector and drying chamber. Minimum improvement potential was required at mass flow rate of 0.041 kg/s for solar air collector. While minimum improvement potential required for dryer was around 0.03426 kWh for flow rate of 0.051 kg/s.

4. Conclusion

This study presents performance evaluation of a v-groove double pass solar air collector and a solar dryer equipped with that collector. A thermodynamic model has been developed and is validated with the extensive experimental data. Energy, exergy, and economic analysis has been conducted for five different flow rates, 0.021, 0.031, 0.041, 0.051 and 0.061 kg/s, on different days. Main conclusions from this study can be summarised as follow:

- Collector outlet air temperature, thermal efficiency and exergy efficiency predicted through thermodynamic model was compared with experimental results with maximum RMSE of 5.53, 11.56 and 1.22, respectively. These results validate the thermodynamic model developed.
- Outlet air temperature continuously decreased with the increasing mass flow rate while thermal efficiency was increased with the mass flow rate. Maximum predicted and experimental outlet air temperatures achieved were 84.95 °C and 81.03 °C at 0.021 kg/s flow rate, respectively. While maximum thermal efficiency achieved numerically and experimentally was 87.6 % and 88.8 % at 0.061 kg/s mass flow rate, respectively.
- Moisture content and drying rate of apple were also affected by mass flow rate. Increasing mass flow rate enhances the moisture removal from the apple up to optimum mass flow rate. Maximum moisture removed from the apple took place at 0.041 kg/s flow rate with final moisture content of 13.11 % followed by 15.85 %, 15.95 %, 16.02 % and 19.89 % for 0.051 kg/s, 0.061 kg/s, 0.031 kg/s and 0.021 kg/s, respectively.
- Exergy efficiency of the solar air collector increases with increment in mass flow rate up to an optimum flow rate while, exergy efficiency of drying chamber kept on increasing with increase in mass flow rate. Maximum exergy efficiency was 6.66 % at 0.051 kg/s for solar air collector while exergy efficiency for the drying chamber was 44.14 % at 0.061 kg/s. Maximum daily average exergy efficiency was 4.49 % at 0.041 kg/s for solar air collector.

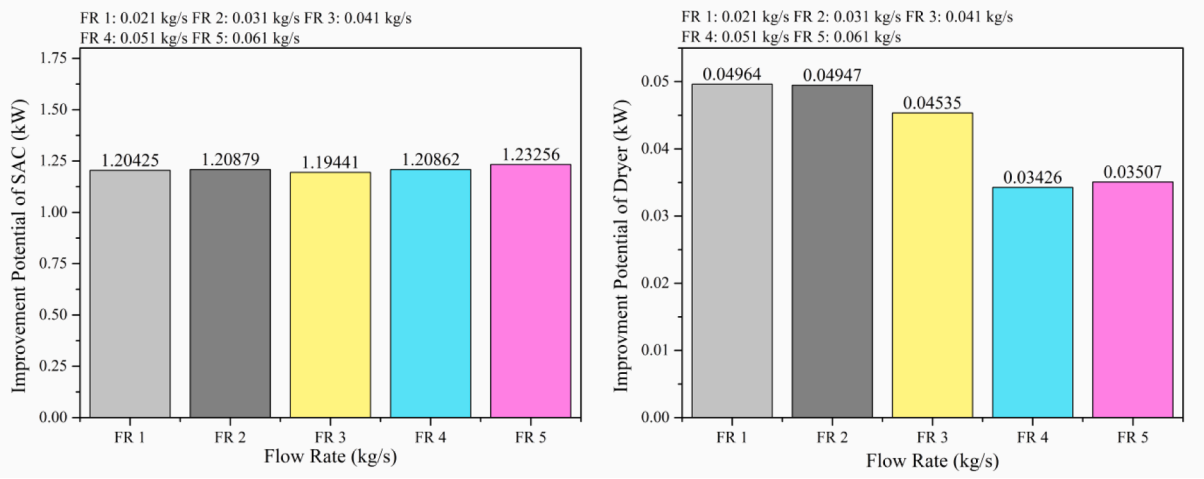

Fig. 16. Improvement potenital of SAC and Dryer at different mass flow rates.

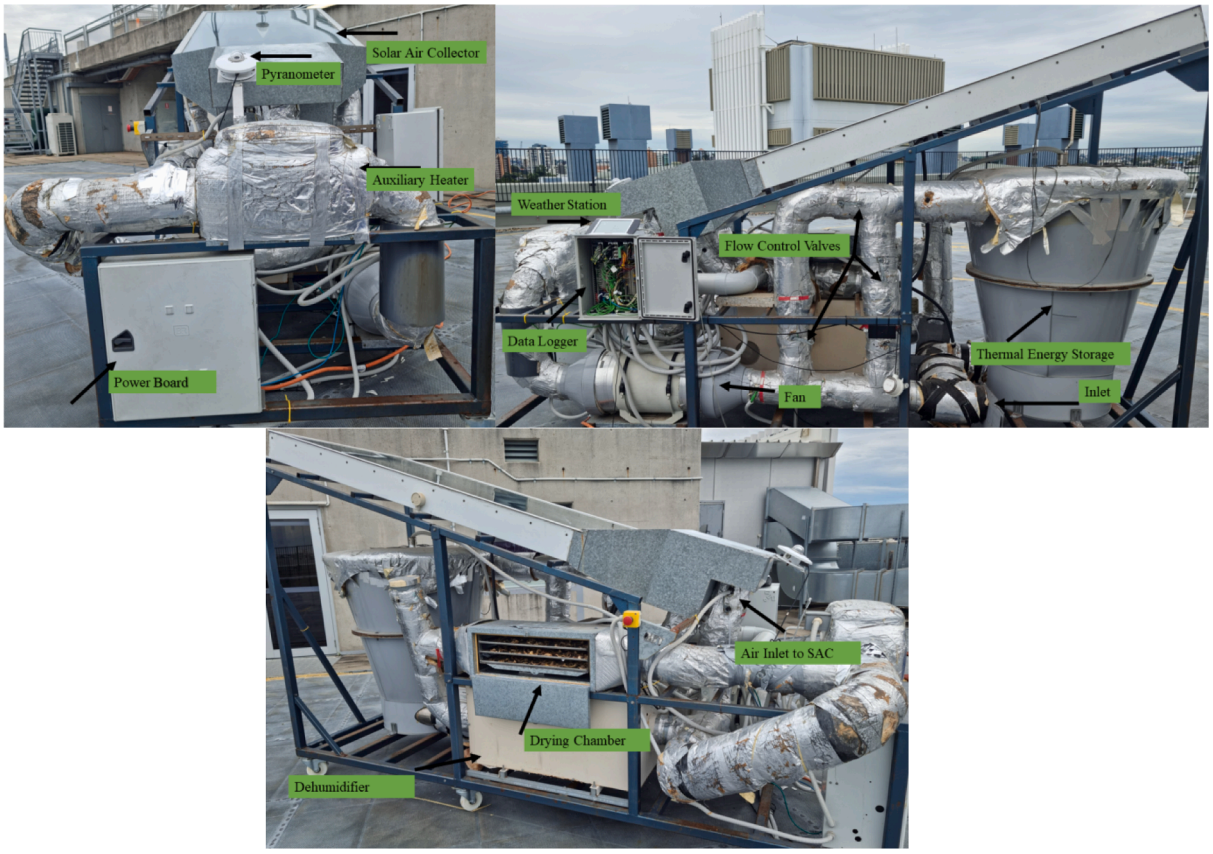

Fig. A1. Experimental Setup.

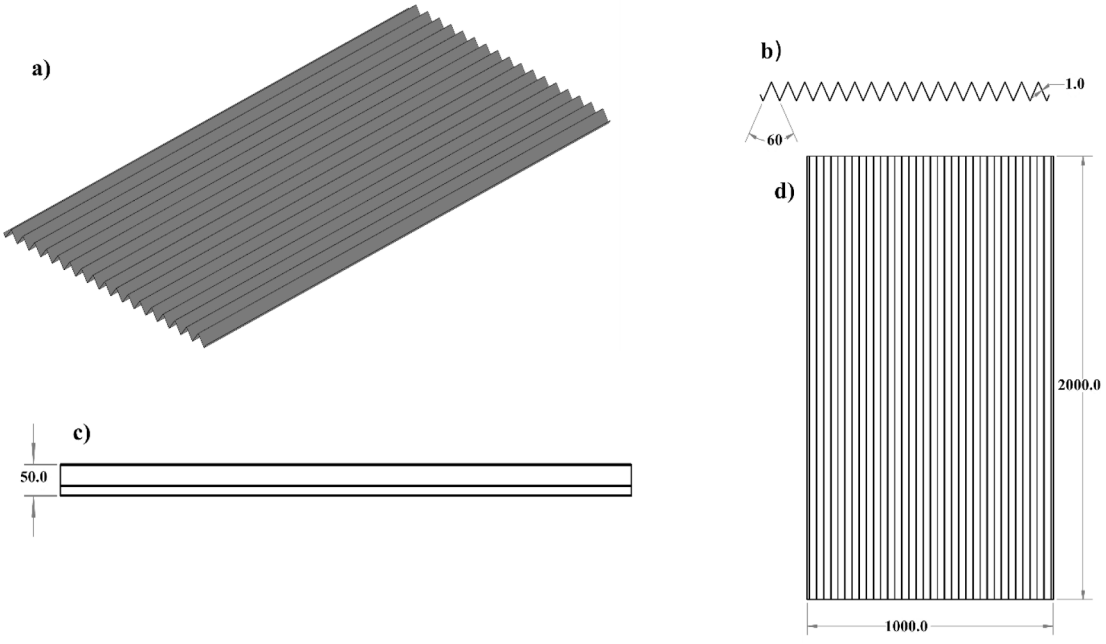

Fig. A2. a) V-Groove absorber plate b) V-groove dimensions c) Side view of v-groove absorber with groove height d) length and width of v-groove absorber.

- Analysing the system by specific energy consumption revealed that solar dryer at the current research has 59 % less annual energy consumption compared to the non-renewable equivalent system.
- Solar air collector and drying chamber have sustainability index of 1.037 % at 0.041 kg/s and 1.50 % at 0.061 kg/s, respectively. Collector performance is significantly affected by high heat losses to the environment, frictional losses and pressure drop in the collector system and therefore there is a high potential for improvement by addressing these losses. Maximum improvement potential for SAC was 1.23 kW at 0.061 kg/s and 0.049 kW for drying chamber at 0.021 kg/s, respectively.

- Energy payback time for the drying system is calculated to be 0.78 years. This implies that the system is feasible from the perspective of life cycle energy management. However, the embodied energy of the solar collector and dryer revealed that the large impact of metals in EE can be mitigated with selection of copper in the absorber plate.

From results, it can be concluded that 0.041 kg/s flow rate is suitable for drying application using solar air dryer as solar air collector had better performance at this flow rate and drying rate of apple was also high compared to other mass flow rate. The performance of V-groove solar air collector can also be further enhanced by optimizing the design configuration of the SAC. One option is to study the effect of jet plate in a V-groove absorber to analyse its energetic and exergetic performance and compare it with V-groove solar air collector.

Declaration of Competing Interest

The authors declare that they have no known competing financial interests or personal relationships that could have appeared to influence the work reported in this paper.

Data availability

Data will be made available on request.

Acknowledgment

The authors acknowledge the support of Dr Sara Omrani, from Queensland University of Technology in providing the long-term solar radiation dataset. Support from the ARC Grants (LP200100493 and DP220103668) are gratefully acknowledged.

References

[1] Kim B, Neff R. Measurement and communication of greenhouse gas emissions from US food consumption via carbon calculators. Ecol Econ 2009;69(1):186–96.
[2] Pham ND, Khan M, Karim M. A mathematical model for predicting the transport process and quality changes during intermittent microwave convective drying. Food Chem 2020:126932.
[3] Kumar C, et al. Temperature redistribution modelling during intermittent microwave convective heating. Procedia Eng 2014;90:544–9.
[4] Duc Pham N, et al. Quality of plant-based food materials and its prediction during intermittent drying. Crit Rev Food Sci Nutr 2019;59(8):1197–211.
[5] Khan MIH, et al. Modelling of simultaneous heat and mass transfer considering the spatial distribution of air velocity during intermittent microwave convective drying. Int J Heat Mass Transf 2020;153:119668.
[6] Kumar C, et al. A porous media transport model for apple drying. Biosyst Eng 2018; 176:12–25.
[7] Khan MIH, et al. Fundamental Understanding of Cellular Water Transport Process in Bio-Food Material during Drying. Sci Rep 2018;8(1):15191.
[8] Mujumdar AS. *Handbook of industrial drying*. 2006: CRC press.
[9] Chua K, et al. Convective drying of agricultural products. Effect of continuous and stepwise change in drying air temperature. Drying Technol 2001;19(8):1949–60.
[10] Arthur O, Karim M. An investigation into the thermophysical and rheological properties of nanofluids for solar thermal applications. Renew Sustain Energy Rev 2016;55:739–55.
[11] EL-Mesery, H.S., et al. Recent developments in solar drying technology of food and agricultural products: A review. Renew Sustain Energy Rev 2022;157:112070.
[12] Karim A, Burnett A, Fawzia S. *Investigation of stratified thermal storage tank performance for heating and cooling applications.* Energies, 2018. **11**(5): p. Article number-1049.
[13] Karim M. Experimental investigation of a stratified chilled-water thermal storage system. Appl Therm Eng 2011;31(11):1853–60.
[14] Karim M, et al. Performance investigation of high temperature application of molten solar salt nanofluid in a direct absorption solar collector. Molecules 2019; 24(2):285.
[15] Karim M, et al. Performance of Graphite-Dispersed Li2CO3-K2CO3 Molten Salt Nanofluid for a Direct Absorption Solar Collector System. Molecules 2020;25(2): 375.
[16] Sun C, et al. A mathematical model to investigate on the thermal performance of a flat plate solar air collector and its experimental verification. Energy Convers Manage 2016;115:43–51.
[17] Bagga GS. Analysis of Flat Plate Solar Air Collector in Different Convection Mode with Induced Turbulence. Int J Eng Res Technol 2016;5(7):488–94.
[18] Mahmood A, Aldabbagh L, Egelioglu F. Investigation of single and double pass solar air heater with transverse fins and a package wire mesh layer. Energy Convers Manage 2015;89:599–607.
[19] Hachemi A. Thermal performance enhancement of solar air heaters, by a fan-blown absorber plate with rectangular fins. Int J Energy Res 1995;19(7):567–77.
[20] Chabane F, Moummi N, Benramache S. Experimental study of heat transfer and thermal performance with longitudinal fins of solar air heater. J Adv Res 2014;5 (2):183–92.
[21] Yang M, et al. Design and optimization of a solar air heater with offset strip fin absorber plate. Appl Energy 2014;113:1349–62.
[22] Saravanakumar P, Somasundaram D, Matheswaran M. Exergetic investigation and optimization of arc shaped rib roughened solar air heater integrated with fins and baffles. Appl Therm Eng 2020;175:115316.
[23] Wang D, et al. Evaluation of the performance of an improved solar air heater with "S" shaped ribs with gap. Sol Energy 2020;195:89–101.
[24] Alam T, Kim M-H. Heat transfer enhancement in solar air heater duct with conical protrusion roughness ribs. Appl Therm Eng 2017;126:458–69.
[25] Bayrak F, Oztop HF, Hepbasli A. Energy and exergy analyses of porous baffles inserted solar air heaters for building applications. Energy Build 2013;57:338–45.
[26] El-Said EM. Numerical investigations of fluid flow and heat transfer characteristics in solar air collector with curved perforated baffles. Engineering Reports 2020;2 (4):e12142.
[27] Fiuk JJ, Dutkowski K. Experimental investigations on thermal efficiency of a prototype passive solar air collector with wavelike baffles. Sol Energy 2019;188: 495–506.
[28] Desisa DG, Shekata GD. Performance Analysis of Flat-Plate and V-groove Solar Air Heater Through CFD Simulation. International Journal of Renewable Energy Development 2020;9(3).
[29] Ho C-D, et al. Efficiency of recycling double-pass V-corrugated solar air collectors. Energies 2017;10(7):875.
[30] El-Sebaii A, et al. Investigation of thermal performance of-double pass-flat and v-corrugated plate solar air heaters. Energy 2011;36(2):1076–86.
[31] Salih MMM, Alomar OR, Yassien HNS. Impacts of adding porous media on performance of double-pass solar air heater under natural and forced air circulation processes. Int J Mech Sci 2021;210:106738.
[32] Abo-Elfadl S, Yousef MS, Hassan H. Energy, exergy, and enviroeconomic assessment of double and single pass solar air heaters having a new design absorber. Process Saf Environ Prot 2021;149:451–64.
[33] Kalaiarasi G, Velraj R, Swami MV. Experimental energy and exergy analysis of a flat plate solar air heater with a new design of integrated sensible heat storage. Energy 2016;111:609–19.
[34] Benhamza A, et al. Multi-objective design optimization of solar air heater for food drying based on energy, exergy and improvement potential. Renewable Energy 2021;169:1190–209.
[35] Islam M, et al. Investigation of the effect of physical and optical factors on the optical performance of a parabolic trough collector. Energies 2017;10(11):1907.
[36] Islam M, Yarlagadda P, Karim A. Effect of the Orientation Schemes of the Energy Collection Element on the Optical Performance of a Parabolic Trough Concentrating Collector. Energies 2018;12(1):1–20.
[37] Karim MA, Hawlader M. Performance investigation of flat plate, v-corrugated and finned air collectors. Energy 2006;31(4):452–70.
[38] Karim M, Hawlader M. Development of solar air collectors for drying applications. Energy Convers Manage 2004;45(3):329–44.
[39] Promvonge P, Skullong S. Heat transfer in solar receiver heat exchanger with combined punched-V-ribs and chamfer-V-grooves. Int J Heat Mass Transf 2019; 143:118486.
[40] Sudhakar P, Cheralathan M. Thermal performance enhancement of solar air collector using a novel V-groove absorber plate with pin-fins for drying agricultural products: an experimental study. J Therm Anal Calorim 2020;140(5):2397–408.
[41] Sethi CK, et al. Exergy, energy and economic analysis of a V-groove assist rotating tray type solar cabinet dryer for drying potato chips. J Stored Prod Res 2021;93: 101861.
[42] Lingayat A, et al. Development of indirect type solar dryer and experiments for estimation of drying parameters of apple and watermelon. Thermal Science and Engineering Progress 2020;16:100477.
[43] Dinçer İ, Zamfirescu C. *Drying phenomena: theory and applications*. 2016: John Wiley & Sons.
[44] Bejan A. *Advanced engineering thermodynamics*. 2016: John Wiley & Sons.
[45] Kumar D, Mahanta P, Kalita P. Performance analysis of a solar air heater modified with zig-zag shaped copper tubes using energy-exergy methodology. Sustainable Energy Technol Assess 2021;46:101222.
[46] Afshari F, et al. Experimental and numerical analysis of a compact indirect solar dehumidification system. Sol Energy 2021;226:72–84.
[47] Lingayat A, Chandramohan V, Raju V. Energy and exergy analysis on drying of banana using indirect type natural convection solar dryer. Heat Transfer Eng 2020; 41(6–7):551–61.
[48] Simo-Tagne M, et al. Energy, environmental and economic analyses of an indirect cocoa bean solar dryer: A comparison between natural and forced convections. Renewable Energy 2022;187:1154–72.
[49] Tuncer AD, et al. Thermal performance analysis of a quadruple-pass solar air collector assisted pilot-scale greenhouse dryer. Sol Energy 2020;203:304–16.
[50] Rahman MM, Joardder MU, Karim A. Non-destructive investigation of cellular level moisture distribution and morphological changes during drying of a plant-based food material. Biosyst Eng 2018;169:126–38.

[51] Moussaoui H, et al. Application of solar drying on the apple peels using an indirect hybrid solar-electrical forced convection dryer. Renewable Energy 2021;168:131–40.
[52] Romano G, Kocsis L, Farkas I. Analysis of energy and environmental parameters during solar cabinet drying of apple and carrot. Drying Technol 2009;27(4):574–9.
[53] Ekka JP, Palanisamy M. Performance assessments and techno and enviro-economic analyses on forced convection mixed mode solar dryer. J Food Process Eng 2021;44(5):e13675.
[54] Lakshmi D, et al. Performance analyses of mixed mode forced convection solar dryer for drying of stevia leaves. Sol Energy 2019;188:507–18.
[55] Hadibi T, et al. Effect of ventilated solar-geothermal drying on 3E (exergy, energy, and economic analysis), and quality attributes of tomato paste. Energy 2022;243:122764.
[56] Gupta A, et al. Sustainability and 4E analysis of novel solar photovoltaic-thermal solar dryer under forced and natural convection drying. Renewable Energy 2022;188:1008–21.
[57] Singh S, et al. A novel active-mode indirect solar dryer for agricultural products: Experimental evaluation and economic feasibility. Energy 2021;222:119956.
[58] Rojas D, et al. Thermal performance testing of flat-plate collectors. Sol Energy 2008;82(8):746–57.
[59] *Agricultural Commodities, Australia, 2019-20 financial year | Australian Bureau of Statistics (abs.gov.au)*. 2019-20.
[60] Kalogirou SA. *Solar energy engineering: processes and systems*. 2013: Academic press.
[61] Duffie JA, Beckman WA. Solar engineering of thermal processes. New York: Wiley; 1980.
[62] Hollands K, Shewen E. *Optimization of flow passage geometry for air-heating, plate-type solar collectors*. 1981.
[63] Karim M, Perez E, Amin ZM. Mathematical modelling of counter flow v-grove solar air collector. Renewable Energy 2014;67:192–201.
[64] ElGamal R, et al. Incorporation of a solar tracking system for enhancing the performance of solar air heaters in drying apple slices. Renewable Energy 2021;167:676–84.
[65] Kesavan S, Arjunan T, Vijayan S. Thermodynamic analysis of a triple-pass solar dryer for drying potato slices. J Therm Anal Calorim 2019;136(1):159–71.
[66] Fudholi A, et al. Performance analysis of solar drying system for red chili. Sol Energy 2014;99:47–54.
[67] Kline SJ. Describing uncertainty in single sample experiments. Mech Engineering 1953;75:3–8.
[68] Daliran A, Ajabshirchi Y. Theoretical and experimental research on effect of fins attachment on operating parameters and thermal efficiency of solar air collector. Information Processing in Agriculture 2018;5(4):411–21.
[69] Matheswaran M, Arjunan T, Somasundaram D. Analytical investigation of solar air heater with jet impingement using energy and exergy analysis. Sol Energy 2018;161:25–37.
[70] Karim MA, Hawlader M. Performance evaluation of a v-groove solar air collector for drying applications. Appl Therm Eng 2006;26(1):121–30.
[71] Das M, Akpinar EK. Determination of thermal and drying performances of the solar air dryer with solar tracking system: Apple drying test. Case Studies in Thermal Engineering 2020;21:100731.
[72] Akbulut A, Durmuş A. Energy and exergy analyses of thin layer drying of mulberry in a forced solar dryer. Energy 2010;35(4):1754–63.
[73] Mugi VR, Chandramohan V. Energy, exergy and economic analysis of an indirect type solar dryer using green chilli: A comparative assessment of forced and natural convection. Thermal Science and Engineering Progress 2021;24:100950.
[74] Vijayan S, Arjunan T, Kumar A. Exergo-environmental analysis of an indirect forced convection solar dryer for drying bitter gourd slices. Renewable Energy 2020;146:2210–23.
[75] *Australian Energy Regulator*: https://www.aer.gov.au/.
[76] Standardization, I.O.f., *Environmental management: life cycle assessment; Principles and Framework*. 2006: ISO.
[77] Dissanayake D, Jayasinghe C, Jayasinghe M. A comparative embodied energy analysis of a house with recycled expanded polystyrene (EPS) based foam concrete wall panels. Energy Build 2017;135:85–94.
[78] Madhankumar S, Viswanathan K, Wu W. Energy, exergy and environmental impact analysis on the novel indirect solar dryer with fins inserted phase change material. Renewable Energy 2021;176:280–94.
[79] Ardente F, et al. Life cycle assessment of a solar thermal collector: sensitivity analysis, energy and environmental balances. Renewable Energy 2005;30(2):109–30.
[80] Mugi VR, Chandramohan V. Energy, exergy, economic and environmental (4E) analysis of passive and active-modes indirect type solar dryers while drying guava slices. Sustainable Energy Technol Assess 2022;52:102250.